JBC RESEARCH ARTICLE

The P53–P21–RB1 pathway promotes BRD4 degradation in liver cancer through USP1

Received for publication, October 2, 2023, and in revised form, January 10, 2024 Published, Papers in Press, February 1, 2024,
https://doi.org/10.1016/j.jbc.2024.105707

Neng Li[1,‡], Erlei Zhang[2,3,‡], Zhenyong Li[1], Suli Lv[1], Xuefeng Zhao[1], Qian Ke[1], Qingli Zou[1], Wensheng Li[1], Yifei Wang[1], Haocheng Guo[1], Tanjing Song[1,4,*], and Lidong Sun[1,4,*]

From the [1]Department of Biochemistry and Molecular Biology, School of Basic Medicine, Tongji Medical College, Huazhong University of Science and Technology, Wuhan, China; [2]Hepatic Surgery Center, Tongji Hospital, Tongji Medical College Huazhong University of Science and Technology, Wuhan, Hubei, China; [3]Key Laboratory of Organ Transplantation, Chinese Academy of Medical Sciences, Wuhan, Hubei, China; [4]Cell Architecture Research Institute, Huazhong University of Science and Technology, Wuhan, Hubei, China

Reviewed by members of the JBC Editorial Board. Edited by Brian D. Strahl

Liver cancer is notoriously refractory to conventional therapeutics. Tumor progression is governed by the interplay between tumor-promoting genes and tumor-suppressor genes. BRD4, an acetyl lysine–binding protein, is overexpressed in many cancer types, which promotes activation of a pro-tumor gene network. But the underlying mechanism for BRD4 overexpression remains incompletely understood. In addition, understanding the regulatory mechanism of BRD4 protein level will shed insight into BRD4-targeting therapeutics. In this study, we investigated the potential relation between BRD4 protein level and P53, the most frequently dysregulated tumor suppressor. By analyzing the TCGA datasets, we first identify a strong negative correlation between protein levels of P53 and BRD4 in liver cancer. Further investigation shows that P53 promotes BRD4 protein degradation. Mechanistically, P53 indirectly represses the transcription of USP1, a deubiquitinase, through the P21–RB1 axis. USP1 itself is also overexpressed in liver cancer and we show USP1 deubiquitinates BRD4 *in vivo* and *in vitro*, which increases BRD4 stability. With cell proliferation assays and xenograft model, we show the pro-tumor role of USP1 is partially mediated by BRD4. With functional transcriptomic analysis, we find the USP1–BRD4 axis upholds expression of a group of cancer-related genes. In summary, we identify a functional P53–P21–RB1–USP1–BRD4 axis in liver cancer.

Liver cancer presents a major challenge to human health world-widely, which claims over 800,000 deaths each year, ranking second among all cancer types (1). Liver cancer is notoriously refractory to conventional radiotherapy and chemotherapy (2). Further understanding of its etiology holds promise for innovative diagnostics and therapeutics. Cancer progression relies on activation and/or overexpression of cancer driver genes. BRD4 has been recognized as a master activator of these cancer driver genes. BRD4 recognizes acetyl-histone through its bromodomain in the N terminus (3). Meanwhile, BRD4 interacts with gene-specific transcription factors and general transcription machinery including mediators (3). BRD4 binds to either promoter or enhancer elements, promoting the transcription of cancer driver genes through engaging with other proteins (3). The target genes of BRD4 vary among cell types and carry out different functions (3), including cell proliferation, metabolism, and immune escape. As a result, BRD4 has risen as a promising therapeutic target with multiple clinical trials carried out or underway. Innovative regimes targeting BRD4 including more potent/specific inhibitors and degradation-inducing agents are under active investigation (4). In cancer, BRD4 mutation is rare while its overexpression is often seen (5–7). BRD4 overexpression contributes to various aspects of cancer malignancy (3). In addition, the level of BRD4 correlates with the cellular sensitivity to BRD4 bromo-domain inhibitors (8–11). These evidence highlight the importance of investigating the regulatory mechanisms of BRD4 expression. Previous studies have established ubiquitin-proteasome–mediated degradation as a critical mechanism regulating BRD4 protein level (12). Ubiquitination, which could tag proteins for proteasomal degradation, is dynamically regulated by two groups of counteracting enzymes (13, 14). On one hand, ubiquitination is catalyzed by the E1, E2, and E3 cascade (14). On the other hand, ubiquitination can be removed by deubiquitinases (13). For BRD4, CULLIN3-RING-SPOP was identified as an E3 ligase while SPOP suffers from inactivating mutation in 9% of prostate cancer (8–10). In contrast, deubiquitinases DUB3 and UCHL3 were reported to reverse BRD4 ubiquitination in prostate cancer and colorectal cancer, respectively (11, 15). In addition, deubiquitinase USP22 was also shown to regulate BRD4 expression (16). But how BRD4 gets overexpressed in most cancers including liver cancer still remains elusive.

P53, encoded by the gene *TP53*, is a well-known tumor suppressor. WT P53 protein has a short half-life under normal conditions and becomes stabilized under various stresses including DNA damage. Due to its master role in control of cell cycle and programmed cell death after DNA damage, P53

‡ These authors contributed equally to this work.
* For correspondence: Tanjing Song, SongT@hust.edu.cn; Lidong Sun, LidongSun@hust.edu.cn.

is widely dubbed the "Guardian of the Genome". However, *TP53* is also the most frequently dysregulated tumor suppressor gene across many cancer types including liver cancer (17). P53 suffers from various inactivating mechanisms, among which, the most common is inactivating mutation. Other mechanisms include accelerated degradation or inhibitory protein–protein interaction. Transcription activation is the prototypical function of WT P53 (18). P53 protein can bind to promoters of a spectrum of target genes, leading to gene activation and various downstream effects, including DNA damage repair, cell cycle arrest, and programmed cell death (18). While P53 itself is recognized as a transcription activator (18), it can also trigger gene repression indirectly. An executor of such effect is the P21–RB axis (19). P21 is encoded by the *CDKN1A* gene, a classic target and effector of P53. P21 potently inhibits cyclin-dependent kinases (CDK) including CDK4/5, CDK2, and CDK1 (19). Through inhibiting CDKs, P21 can then activate another group of tumor suppressors, the RB family, which would otherwise be phosphorylated and inactivated by CDKs (19). When activated, the RB family members, RB1/p105, RBL1/p107, and RBL2/p130 form protein complexes with E2F factors (19). RB family members not only abolish the transcription activation by E2F factors but also nucleate complexes actively repressing the E2F target genes. Two different transcription-repressive protein complexes are known to form (19), the RB-E2F complex and the DREAM complex. While the RB–E2F complex contains RB1/P105, the DREAM complex is formed by P107 or P130 together with other common subunits including LIN37 (19). The RB–E2F and DREAM complexes may function cooperatively downstream P53–P21 axis to inhibit cell cycle progression (20, 21). However, whether and how P53 or the P21–RB axis affects BRD4 expression was unknown.

In this study, our analysis reveals the P53 protein levels exhibit significant negative correlation with the BRD4 protein levels in liver cancer. We show that P53 represses BRD4 protein stability. Mechanistically, we identify USP1 as a deubiquitinase for BRD4 and transcription of USP1 is repressed by P53 via the P21–RB1 axis. Through transcriptomic analysis, we uncover that the USP1–BRD4 axis promotes liver cancer cell proliferation through upregulating a group of cancer-related genes.

Results

P53 decreases BRD4 protein stability

We are interested in the regulation of BRD4 expression in liver cancer due to several observations. Firstly, BRD4 protein is overexpressed in liver cancer (22, 23). Secondly, higher BRD4 protein level correlates with worse overall survival in liver cancer patients (22–25). Thirdly, after knocking down BRD4, we detected a significant decrease in cell proliferation with both CCK-8 and clonogenesis assays (Fig. S1, *A* and *B*), which is consistent with previous reports in other liver cancer cell lines (23, 25, 26). To explore the potential link between BRD4 and P53, we started by analyzing whether correlation existed between their protein levels in human liver cancer (refer to the hepatocellular carcinoma cohort hereafter) with the antibody-based TCGA (The Cancer Genome Atlas) RPPA (reverse phase protein array) dataset. We found a strong and statistically significant negative correlation between the protein levels of P53 and BRD4 in 121 *TP53*-WT cancer samples (Pearson coefficient r=−0.697, p = 6.5e-19) (Fig. 1*A*). In addition, the BRD4 protein level is higher in P53-mutant samples than in P53-WT samples in the TCGA liver cancer cohort (Fig. S1*C*). Besides liver cancer, negative correlation between the protein levels of BRD4 and WT P53 was also observed in 16 other TCGA cancer types (Table S1). In contrast, none cancer type showed a positive correlation (Table S1). To examine whether P53 might regulate BRD4, we overexpressed P53 in liver cancer cells. Acute P53 expression induced by doxycycline decreased BRD4 protein levels in HLF, HLE, and HepG2 liver cancer cells (Figs. 1*B* and S1*D*). To corroborate this repressive effect of P53 on BRD4, we knocked-down P53 in HepG2 cancer cells, which expresses WT P53 according to The Cancer Cell Line Encyclopedia (27). Western blot (WB) detected increased BRD4 protein level after P53 knock-down (Fig. 1*C*). To determine whether regulation of BRD4 plays a role in P53 functions, we knocked-down BRD4 in P53 knock-down cells. Cell counting and clonogenesis showed BRD4-KD ameliorated cell growth induced by P53-KD, indicating downregulation of BRD4-mediated part of P53 function (Fig. S1, *E* and *F*). Hence we set out to investigate how P53 regulated BRD4. We first performed realtime RT-PCR, which showed BRD4 mRNA level was not significantly changed by P53 (Fig. S1*G*). We then examined whether BRD4 protein stability was by P53. Cycloheximide (Chx) was used to block cell protein synthesis to monitor BRD4 protein decay. Navtemadlin, an MDM2 inhibitor, was used to treat cells to increase the endogenous P53 level. The result showed BRD4 protein stability was indeed decreased by Navtemadlin (Fig. 1*D*). Consistently, BRD4 protein stability was also decreased by P53 overexpression while increased by P53 knock-down in liver cancer cells (Fig. 1, *E* and *F*). Ubiquitin-proteasomal system plays a pivotal role in regulating the stability of proteins including BRD4. To examine whether it was involved in the regulation of BRD4 by P53, we used MG132 to block proteasome-mediated degradation. The result showed MG132 diminished the effect of P53 on BRD4 protein level (Figs. 1*G* and S1*H*), which indicated proteasome was required for regulation of BRD4 by P53. We went on to examine whether BRD4 ubiquitination was regulated by P53 with immunoprecipitation (IP)-WB. BRD4-KD cells were included as control to show the specificity of ubiquitination signals. The results showed BRD4 ubiquitination level was decreased by P53-KD while increased by P53-OE (Fig. 1, *H* and *I*). These results altogether showed that P53 promoted ubiquitination-proteasomal degradation of BRD4 in liver cancer.

BRD4 interacts with USP1

We next set out to uncover how P53 regulates BRD4 ubiquitination. Protein ubiquitination is mainly controlled by counteracting E3 ligase and deubiquitinase. As the

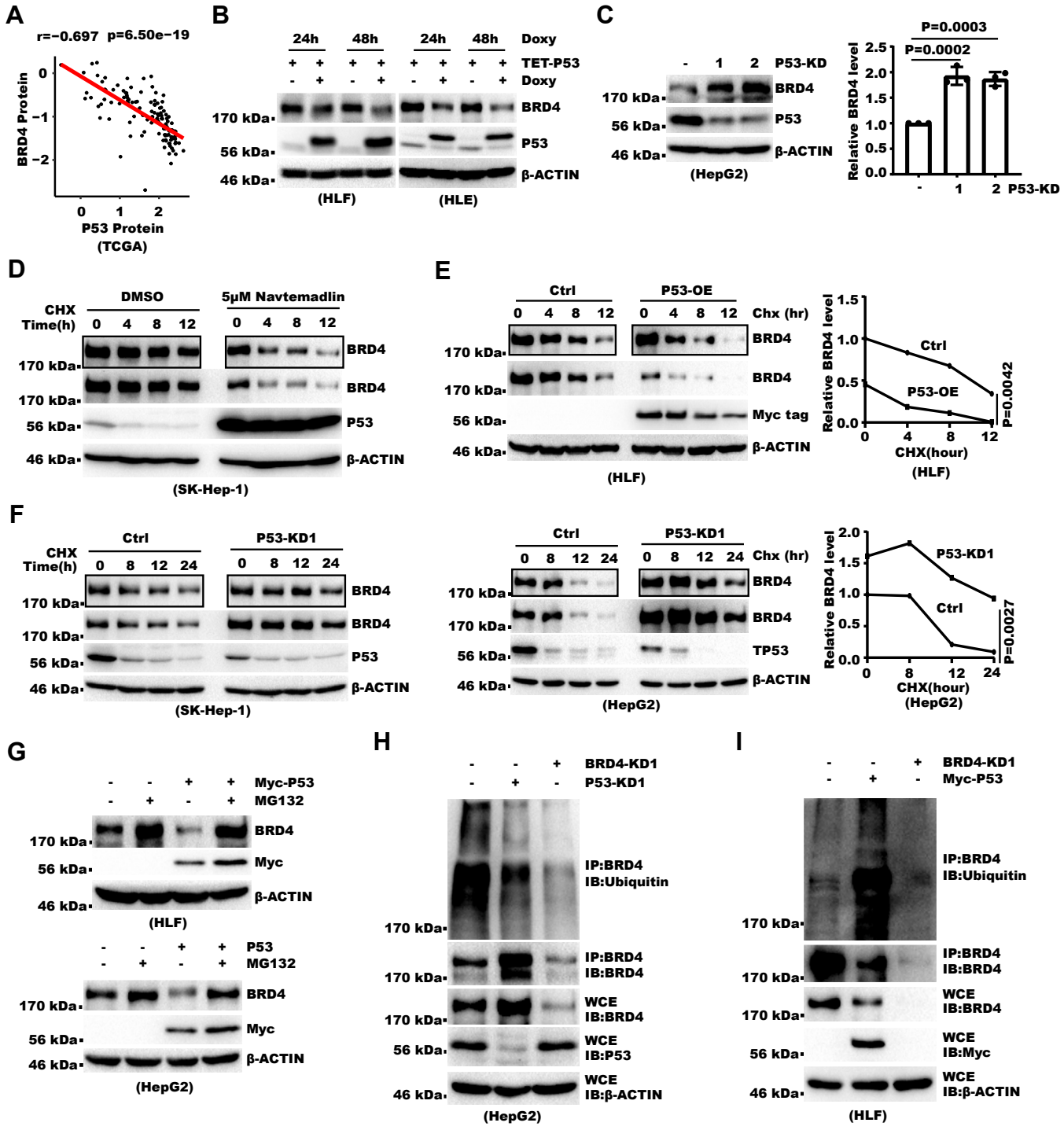

Figure 1. P53 decreases BRD4 protein stability. *A*, shown is linear regression analysis for P53 and BRD4 protein levels in 126 P53-WT patients from TCGA liver cancer (hepatocellular carcinoma) cohort. The "r" denotes Pearson correlation coefficient. *B*, P53-WT were expressed with tetracycline (TET)/doxycycline (Doxy)-inducible vector in HLF and HLE cells. Cells were treated with doxycycline for 24 h and 48 h as indicated before harvest. WCL were then analyzed with Western Blot. *C*, P53 was knocked down in HepG2 cells with lentivirus-expressed shRNA. WCL were analyzed with WB. Shown on the *left* are WB images. Shown on the *right* is densitometry analysis of BRD4 level from WB of three biological replicates. BRD4 level is presented as the relative ratio between BRD4 and β-ACTIN. Error bars denote SD and *p* value was calculated from Student's *t* test. *D*, SK-Hep-1 cells were treated with 5 μM Navtemadlin for 24 h. Cells were then treated with 50 μg/ml cycloheximide (Chx) for indicated time. WCL were analyzed with Western blot. *E*, Myc-P53 was overexpressed in HLF cells. Cells were then treated with 50 μg/ml cycloheximide (Chx) for indicated time. WCL were analyzed with Western blot. Shown on the *left* are WB images. Shown on the *right* is densitometry analysis of BRD4 level from WB. BRD4 level is presented as the relative ratio between BRD4 and β-ACTIN. *p* value was calculated from two-way ANOVA. *F*, HepG2 and SK-HEP-1 cells was infected with lentivirus expressing control or *TP53*-shRNA. Cells were treated with 50 μg/ml Chx for indicated time and analyzed with Western blot. Shown on the *left* are WB images. Shown on the *right* is densitometry analysis of BRD4 level from WB. BRD4 level is presented as the relative ratio between BRD4 and β-ACTIN. *p* value was calculated from two-way ANOVA. *G*, control or P53-overexpressing cells were treated with 25 μM MG132 for 8 h before harvest. WCL were then analyzed with WB. *H*, BRD4 was immunoprecipitated from control or *TP53*-KD HepG2 cells followed by WB analysis. BRD4-KD cells were used as a control to validate signal specificity. Cells were treated with 25 μM MG132 for 4 h before harvest. *I*, endogenous BRD4 was immunoprecipitated from control or *TP53*-OE HepG2 cells followed by WB analysis. BRD4-KD cells were used as a control to show signal specificity. Cells were treated with 25 μM MG132 for 4 h before harvest.

prototypical biochemical activity of P53 is transcription activation, we examined whether P53 regulated the mRNA level of known BRD4 E3 ligase or deubiquitinase, including DUB3, SPOP, UCHL3, and USP22 (8–11, 15, 16). However, we failed to detect concordant change in these genes that seemed to explain the change in BRD4 although knocking down UCHL3 or DUB3 decreased BRD4 protein level (Fig. S2, *A* and *B*). So we turned to the possibility that a hitherto unrecognized E3 or deubiquitinase of BRD4 was involved in the regulation of BRD4 by P53. In this regard, Ubiquitin Specific Peptidase 1 (USP1) was previously identified in the immunoprecipitate of BRD4 1-722aa fragment in a proteomic study (28). USP1 is a Ubiquitin specific peptidase (USP)-family deubiquitinase. Like many other deubiquitinases, it is a cysteine protease (13). Yet unlike many other deubiquitinases, USP1 stand-alone is almost inactive. Instead, its activity is dramatically enhanced by an indispensable partner, WDR48 (29, 30), which is also called UAF1, short for USP1-associated factor 1. Interestingly, WDR48 was also identified in the immunoprecipitate of BRD4 in the same proteomic study (28), adding to the confidence in USP1 identification. We hypothesized USP1 might regulate BRD4 ubiquitination. We first examined by immunostaining whether USP1 and BRD4 localized to the same cellular compartment in liver cancer cells. The result showed they both mainly localized to the cell nucleus (Fig. S2*C*). Specificity of the staining signals was validated by their decrease in the USP1-KD and BRD4-KD cells. To further corroborate, we also expressed exogenous-tagged USP1 and BRD4 with lenti-virus and then stained them with anti-tag antibodies. The result confirmed that USP1 and BRD4 mainly localized to the cell nuclei (Fig. S2*D*). After making sure BRD4 and USP1 were not geographically segregated, we examined whether they interacted with each other. The results of coIP showed both exogenous and endogenous USP1 co-immunoprecipitated with BRD4 (Fig. 2, *A* and *B*). To further corroborate, we purified recombinant GST-USP1 and incubated it with the lysate of FLAG-BRD4–expressing cells. GST pull-down experiment showed FLAG-BRD4 was coprecipitated with GST-USP1 (Fig. 2*C*). Similarly, GST-USP1 pulled-down endogenous BRD4 (Fig. 2*D*), confirming the interaction between BRD4 and USP1. Since WDR48 is necessary for USP1 activity, we then included WDR48 in the cotransfection and coIP-WB assay for BRD4 and USP1. The result showed both endogenous and exogenous WDR48 were also immunoprecipitated by BRD4, indicating BRD4 could interact with enzymatically active USP1 (Fig. 2, *E* and *F*). To narrow down which part of BRD4 mediated the interaction with USP1, we generated serial deletion mutants of BRD4. Coprecipitation assay showed 471-730aa region after BRD4's tandem bromodomains interacted with USP1 (Fig. 2, *G* and *H*). Collectively, these data uncover USP1, which physically interacts with BRD4.

USP1 deubiquitinates and stabilizes BRD4

We next asked whether USP1 regulated BRD4 protein stability and mediated P53's effect on BRD4 in liver cancer cells. We first analyzed whether BRD4 correlated with USP1 level in the TCGA liver cancer RPPA dataset. As the dataset does not contain information of USP1 protein level, we used its mRNA level from RNA-seq as a surrogate. Analysis revealed a significant positive correlation between the BRD4 protein levels and USP1 mRNA levels (Fig. S3*A*). To corroborate, we also analyzed protein levels of BRD4 and USP1 by WB in the fresh liver cancer samples and normal samples we collected (Fig. S3*B*). The result confirmed previous reports that BRD4 is overexpressed in liver cancer samples (Fig. S3*C*). Importantly, it showed that BRD4 and USP1 significantly correlated with each other in both liver cancer tissues and normal tissues (Figs. 3*A* and S3*D*). We went on to examine whether USP1 regulated BRD4 protein level. Treating cells with USP1 inhibitor ML323 significantly decreased BRD4 protein level in a dosage-dependent manner (31) (Fig. S3*E*). Consistently, the BRD4 protein level was also decreased by USP1 knock-down with either constitutive or tetracycline-inducible shRNA (Figs. 3*B* and S3, *F*–*H*). Of note, USP1-KD further decreased BRD4 protein level in DUB3-KD cells, indicating USP1 regulates BRD4 independent of DUB3 (Fig. S3*I*). Real-time RT-PCR indicated USP1 did not change BRD4 expression at the mRNA level (Fig. S3*J*). Instead, its protein stability was decreased by USP1-KD as shown by Chx treatment (Figs. 3*C* and S3*K*). Consistently, the decrease in BRD4 was abolished by MG132 treatment, which indicated involvement of the ubiquitination-proteasome pathway (Figs. 3*D* and S3*L*). IP-WB showed that USP1-KD indeed increased ubiquitination of BRD4 in different liver cancer cells (Fig. 3*E*). To determine whether deubiquitinase activity of USP1 was necessary for the regulation of BRD4, we introduced C90S mutation to USP1, which disrupted its catalytic cysteine. The result showed C90S mutant lost effect on BRD4 protein level (Fig. 3, *F* and *G*), indicating deubiquitinase activity of USP1 is necessary. Consistently, overexpressing WDR48 together with USP1 further increased BRD4 protein level compared to overexpressing USP1 alone (Fig. 3*H*). In contrast, WDR48-KD decreased BRD4 protein level (Fig. 3*I*). To examine whether USP1 deubiquitinated BRD4, we then set up *in vivo* and *in vitro* deubiquitination assay. The result showed USP1-WT but not C90S mutant deubiquitinated BRD4 (Fig. 3, *J* and *K*). The specific requirement of USP1 activity in these assays was validated as C90S mutant, as a control, failed to show any effect (Fig. 3, *J* and *K*). These data collectively showed USP1 deubiquitinated BRD4 and promoted its protein stability in liver cancer cells. We then examined whether USP1 had to do with the regulation of BRD4 by P53. Knocking-down USP1 diminished the effect of P53 on BRD4 expression, indicating USP1 was required for BRD4 regulation by P53 (Fig. 3*L*).

BRD4 mediates the pro-proliferation effect of USP1

Having found USP1 promoted BRD4 protein stability in liver cancer cells, we next investigated whether the USP1–BRD4 axis promoted liver cancer cell proliferation. Analysis of the TCGA RNA-Seq data showed USP1 was significantly higher in liver cancer than normal samples (Fig. S4*A*). We further confirmed with WB that USP1 protein level was significantly higher in liver cancer samples than paired normal

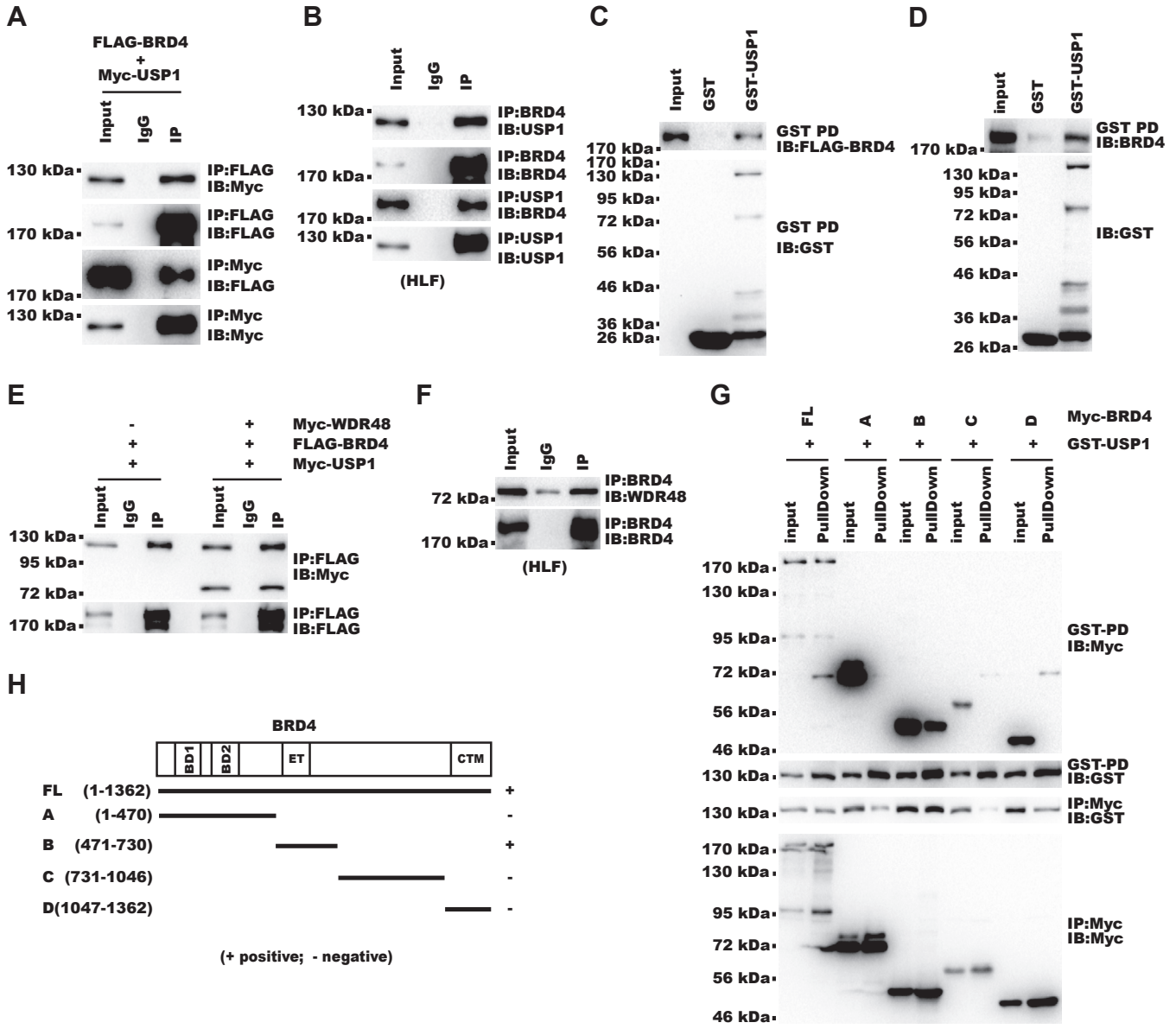

Figure 2. BRD4 interacts with USP1. *A*, Flag-BRD4 and Myc-USP1 were transfected into HEK-293T cells. Cells were analyzed with CoIP-WB. USP1-GG670/671AA was used here to avoid auto cleavage of overexpressed USP1 but does not affect its enzymatic activity (43, 56). *B*, CoIP-WB for endogenous BRD4 and USP1 in HLF cells. *C*, Flag-BRD4 was transfected into HEK-293T cells. Whole cell lysate was then incubated with recombinant GST-USP1 with GST as control. Glutathione-beads pulldown was analyzed with WB. *D*, HLF whole cell lysate was incubated with recombinant GST-USP1 with GST as control. Glutathione-beads pulldown was analyzed with WB. *E*, Flag-BRD4, Myc-WDR48, and Myc-USP1 were cotransfected into HEK-293T cells. Shown are results of coIP–WB. USP1-GG670/671AA was used here to avoid auto cleavage of overexpressed USP1 but does not affect its enzymatic activity (43, 56). *F*, CoIP-WB for endogenous BRD4 and WDR48 in HLF cells. *G*, GST-USP1 and a set of Myc-BRD4 fragments were cotransfected into HEK-293T cells. Cells were then subject to co-IP or GST-pulldown followed by WB analysis. *H*, the schematic diagram illustrates Myc-BRD4 expression constructs and their ability to interact with USP1 as examined in (*G*). "+" indicates ability to interact with GST-USP1 while "-" indicates otherwise.

samples (Fig 4*A*). Survival analysis showed USP1 mRNA level correlated with poor survival in the TCGA dataset (Fig. S4*B*). To examine whether USP1 overexpression contributed to cell proliferation like BRD4, we knocked-down USP1 and performed both CCK8 and clonogenesis assays. The result showed liver cancer cell proliferation was significantly inhibited by USP1-KD (Fig. S4, *C* and *D*). To examine whether BRD4 contributed to the pro-proliferation effect of USP1, we introduced exogenous BRD4 to restore BRD4 protein level in USP1-KD cells. The result showed cell proliferation was also partially restored (Figs. 4, *B* and *C* and S4, *E* and *F*). To further validate this in an animal model, we inoculated liver cancer cells to immunodeficient mice. The result showed not only USP1-KD significantly inhibited tumor growth (Fig. 4, *D* and *E*) but also restoring BRD4 expression partially restored tumor growth (Fig. 4, *D* and *E*). These data collectively showed USP1 promotes liver cancer cell proliferation partially through BRD4.

The USP1–BRD4 axis promotes expression of cancer-related genes

We showed the USP1–BRD4 axis promoted proliferation of liver cancer cells. To gain insight into the underlying

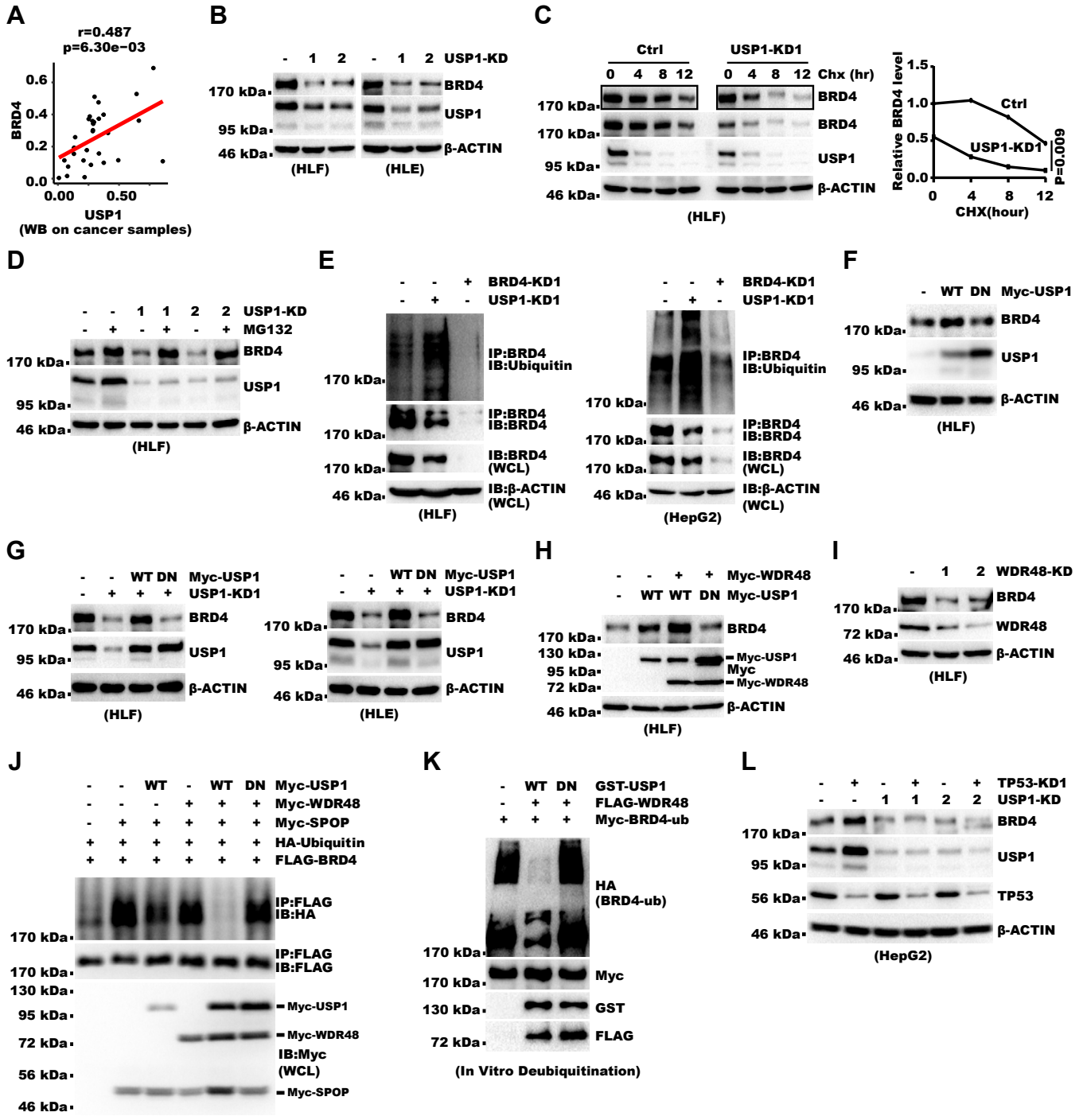

Figure 3. USP1 deubiquitinates and stabilizes BRD4. *A*, linear regression analysis for levels of USP1 and BRD4 in 30 liver cancer tissues. Protein levels detected with WB were first normalized to GAPDH and then to HepG2 on the same gel. The 'r' denotes Pearson correlation coefficient. *B*, USP1 was knocked-down by lentivirus-expressed shRNA. WCL were analyzed with Western Blot. *C*, control or USP1-KD cells were treated with 50 μg/ml Chx for indicated time. Shown on the *left* are WB images. Shown on the *right* is densitometry analysis of BRD4 level from WB. BRD4 level is presented as the relative ratio between BRD4 and β-ACTIN. *p* value was calculated from two-way ANOVA. *D*, control or USP1-KD cells were treated with 25 μM MG132 for 8 h. WCL were analyzed with WB. *E*, endogenous BRD4 was immunoprecipitated from control or USP1-KD HLF cells followed by WB analysis. All cells were treated with 25 μM MG132 for 4 h before harvest. BRD4-KD cells were used as control to validate specificity of signals. *F*, USP1-WT or -C90S (DN) was overexpressed in HLF cells. WCL were analyzed with Western blot. *G*, USP1-WT or -C90S (DN) was rescue-expressed in USP1-KD cells (The shRNA used targets 3′-UTR of USP1 mRNA). WCL were analyzed with WB. *H*, USP1-WT or -C90S (DN) was coexpressed with myc-WDR48 in HLF cells. WCL were analyzed with Western blot. USP1-GG670/671AA was used to avoid auto cleavage of overexpressed USP1 but does not affect its enzymatic activity (43, 56). *I*, WDR48 was knocked-down with lentivirus-expressed shRNA. WCL were analyzed with WB. *J*, plasmids as indicated were transfected into HEK-293T cells. Cells were treated with 25 μM MG132 for 4 h before collection. FLAG antibody immunoprecipitates or WCL were analyzed by WB. *K*, Myc-tagged BRD4 and HA-tagged Ubiquitin were first overexpressed in 293T cells. Cells were treated with 25 μM MG132 for 4 h before collection. Myc-BRD4 was then immunopurified and *in vitro* deubiquitinated. Recombinant GST-USP1-WT or -C90S (DN) from *Escherichia coli* and FLAG-WDR48 immunopurified from transfected 293T cells were added as deubiquitinase. Reactants were analyzed by WB. *L*, *TP53* was knocked-down in control or USP1-KD cells. WCL were analyzed with WB.

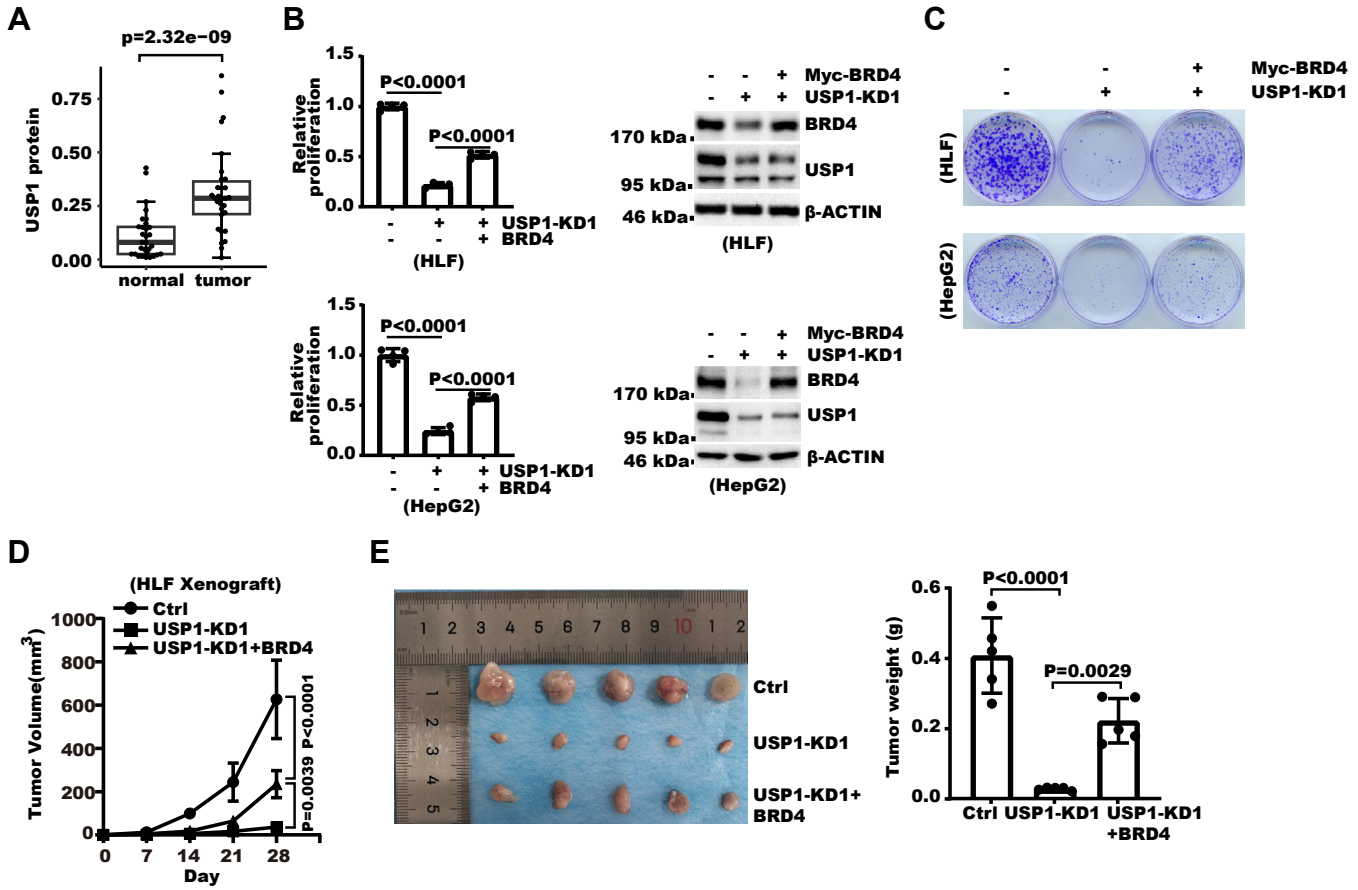

Figure 4. BRD4 mediates pro-proliferation effect of USP1. *A*, the boxplot summarizes the densitometry analysis of Western Blot shown in Fig. S3*B*. USP1 levels shown were first normalized to GAPDH (Fig. S3*B*) and then to HepG2 WCL on the same gel. *p* value was calculated by paired two-sided Welch's *t* test. *B*, USP1 was knocked down and then exogenous BRD4 was rescue expressed. Cell proliferation was then analyzed with cell counting and WCL were analyzed with WB. Shown on the *left* is relative proliferation fold over 6 days. Shown on the *right* are WB results. Error bars denote SD of four biological replicates. *p* values were calculated from one-way ANOVA with correction for multiple comparison. *C*, USP1 was knocked down and then exogenous BRD4 was rescue expressed. Five hundred cells were then seeded into each 3.5-cm dish. Fourteen days later, cell colonies were fixed and stained with crystal violet. *D*, 5 × 10^6 HLF cells as described in (*B* and *C*) were first resuspended in 100 μl 1:1 mixture of PBS and Matrigel. Cells were then injected subcutaneously into flanks of 5- to 6-week-old male BALB/c nude mice. Shown are the growth curves of xenograft. *p* value was calculated with two-way ANOVA followed by pair-wise comparison as indicated. *E*, xenografts from (*D*) were photographed and weighed. Shown on the *left* are xenograft images. Shown on the *right* are summary of tumor weights. Error bars denote SD and *p* values were calculated from one-way ANOVA with correction for multiple comparison.

mechanism, we next analyzed how the USP1–BRD4 axis regulated liver cancer cell transcriptome with RNA-seq, given the major role of BRD4 as a transcription regulator. Knockdown of either USP1 or BRD4 caused significant change in the expression of more than 100 genes (Fig. S5*A*, gene list deposited to GEO). To support the connection between USP1 and BRD4, significant overlap exists between genes downregulated by USP1-KD and genes downregulated by BRD4-KD (Fig. S5*B*, overlapping genes listed in Table S2). Consistently, gene set enrichment analysis (GSEA) analysis showed USP1 and BRD4 also regulated common pathways. Among the top 10 pathways regulated by USP1 and BRD4, respectively, four are common, including hypoxia response and glycolysis, which are known contributors to cancer progression (Fig. 5*A*). To validate the RNA-Seq result, we picked four commonly regulated genes in these pathways for validation, which are *CA9*, *TNS4*, *NDUFA4L2*, and *SLC2A3*. Relevance of these genes with cancer has been reported (32–37). Real-time RT-PCR validated their downregulation after both USP1-KD and BRD4-KD in both HepG2 and HLF cells (Fig. 5*B*). To determine whether these genes are critical for liver cancer cell proliferation, we knocked-down them and detected significant decrease in cell proliferation (Figs. 5*C* and S5*C*). Among genes commonly regulated by USP1 and BRD4, we picked *CA9* to further examine whether it contributed to the pro-proliferation effect of BRD4. *CA9* was picked for several reasons. *CA9* encodes carbonic anhydrase IX, which was known as a key target of HIF1 during the hypoxia response in cancer (32). Survival analysis showed *CA9* mRNA level correlated with poor patient survival in the TCGA liver cancer cohort (Fig. S5*D*). In addition, we found the *CA9* mRNA levels positively correlated with the USP1 and BRD4 protein levels in the TCGA liver cancer cohort (Fig. S5, *E* and *F*). We restored *CA9* expression in BRD4-KD cells and found that cell proliferation was also partially restored (Fig. 5, *D* and *E*). Altogether, these data showed the USP1–BRD4 axis upregulated the expression of cancer-relevant genes which could mediate their proliferation-promoting effect.

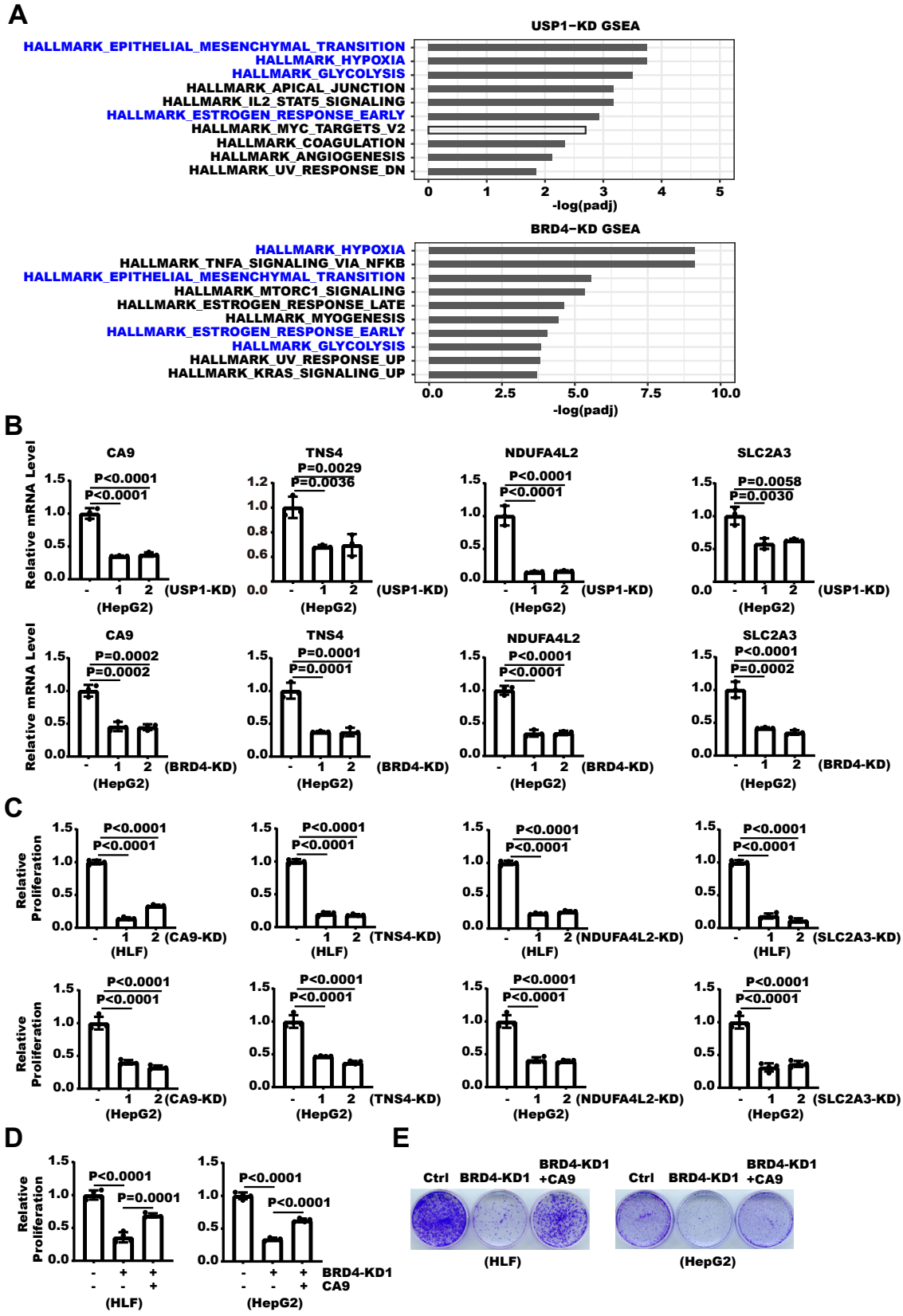

Figure 5. USP1–BRD4 axis promotes expression of cancer-related genes. *A*, shown is GSEA analysis for pathway significantly changed by USP1-KD and BRD4-KD. Filling in *gray* indicates downregulated pathway. *Open* bar indicates upregulated pathways. Pathways with names colored in *blue* are commonly regulated by USP1-KD and BRD4-KD. *B*, USP1-KD or BRD4-KD cells were analyzed with real-time RT-PCR. Error bars denote SD of three technical replicates. *p* values were calculated from one-way ANOVA with correction for multiple comparison. *C*, *CA9*, *TNS4*, *NDUFA4L2*, and *SLC2A3* were knocked down in HLF and HepG2 cells. $6*10^5$ cells were seeded into each 6-cm dish. Cell proliferation over 5 days was analyzed with cell counting. The presented relative proliferation was normalized to that in control cells. Error bars denote SD of four biological replicates. *p* values were calculated with one-way ANOVA followed by pair-

P53 represses USP1 and BRD4 expression through the P21–RB1 axis

We found USP1 was required for the regulation of BRD4 protein stability by P53 (Fig. 3). Next we investigated whether and how P53 might regulate USP1. We found overexpressing P53 decreased USP1 protein level (Figs. 6*A* and S6*A*). Consistently, knocking-down P53 in P53 WT HepG2 and SK-HEP-1 cells increased USP1 protein level (Fig. 6*B*). Consistently, treatment with MDM2 inhibitor Navtemadin also decreased USP1 protein level as well as BRD4 protein level (Fig. 6*C*). After P53 overexpression or knockdown, realtime RT-PCR indicated USP1 was regulated by P53 at the mRNA level (Fig. 6, *D* and *E*). Consistent with our data, analysis of the TCGA liver cancer RNA-seq data and RPPA data also revealed significant negative correlation between the P53 protein levels and the USP1 mRNA levels in P53 WT samples (Fig. 6*F*). In addition, *TP53*-mutant samples expressed significantly higher level of USP1 mRNA than *TP53*-WT ones (Fig. S6*B*). To examine whether P53 repressed USP1 expression at the transcription level, we constructed luciferase reporter plasmid driven by USP1 promoter and stably expressed this construct in liver cancer cells. We found, in these cells, luciferase activity was significantly decreased by P53 overexpression while increased by P53-KD (Figs. 6, *G* and *H* and S6*C*), which supported P53 repressed USP1 transcription. Next, we investigated how P53 triggered repression of USP1 transcription. Increase in USP1 protein after DNA damage was previously shown to be more significant in P21-KO HCT116 cells albeit underlying mechanism was unknown (38). We hypothesized that P21 might repress USP1 expression and mediate the regulation of USP1 by P53. We first knocked-down P21 and detected increase in USP1 with concordant increase in BRD4 (Figs. 6*I* and S6*D*). In contrast, P21 overexpression had opposite effect (Fig. 6*J*). Consistent with regulation at the transcriptional level, USP1 promoter luciferase reporter activity was increased by P21-KD as well (Figs. 6*K* and S6*E*). Importantly, knocking-down P21 diminished the effect of P53 on USP1 and BRD4 expression (Fig. 6*L*). P21 could induce gene repression through two different effectors, the RB-E2F complex and the DREAM complex (19–21). RB1 is indispensable for the RB1-E2F complex while LIN37 is indispensable for the DREAM complex (19–21). We knocked-down RB1 and LIN37 respectively to examine their impact on USP1 and BRD4 expression. The result showed RB1-KD but not LIN37-KD diminished the effect of *TP53* on USP1 and BRD4 (Figs. 6, *M* and *N* and S6, *F*–*H*). RT-PCR showed that RB1-KD increased USP1 expression at the mRNA level (Fig. 6*O*). We then performed chromatin-IP and revealed RB1 bound to the USP1 promoter (Fig. 6*P*). Consistent with the regulation of USP1 by RB1, analysis of the TCGA liver cancer RPPA data and RNA-seq data revealed the RB1 protein levels significantly correlated with the USP1 mRNA levels or BRD4 protein levels (Fig. S6, *I* and *J*). To confirm if RB1 regulated USP1 at the transcriptional level, we knocked-down RB1 in USP1-promoter luciferase reporter cells. The result showed RB1-KD indeed increased the luciferase activity (Fig. 6*Q*). These results showed the P21–RB1 axis repressed USP1 transcription. We went on to confirm whether the P21–RB1 axis mediated regulation of USP1 by P53. We examined the effect of P53 on USP1 expression in P21-KD and RB1-KD cells. The result showed either knockdown diminished the repressive effect of P53 on USP1-promoter reporter (Fig. 6*R*), which supports that P53 represses USP1 transcription through the P21–RB1 axis. Earlier, we identified *CA9* as a functional downstream effector of the USP1–BRD4 axis (Fig. 5). Interestingly, the *CA9* mRNA level was significantly higher in P53-mutant samples than in P53-WT samples from the TCGA liver cancer cohort (Fig. S6*K*). Consistently, the *CA9* mRNA levels also negatively correlated with P53 and RB1 protein levels in P53 WT samples (Fig. S6, *L* and *M*), which is consistent with the finding that P53 repressed USP1 transcription through RB1. Collectively, these data revealed that P53 repressed USP1 transcription and BRD4 expression through the P21–RB1 axis (Fig. 7).

Discussion

P53 decreases BRD4 protein level

The outcome of cancer depends on intricate interplay between different oncogenes and tumor suppressor genes. P53 and BRD4 both function as master regulators of gene transcription and cancer progression. Multilevel interplay between the two is emerging. Firstly, BRD4 potentially interacts with (39) and colocalizes with P53 to certain genomic regions (40). Consistently, BRD4 is required for P53-mediated gene activation of certain target genes including P21 in HEK-293 and HCT116 cells (39). Secondly, although BRD4 has mainly been attributed a transcription-activation function, it was reported to promote gene silencing in some scenarios (41, 42). In acute myeloid leukemia cells, BRD4 can suppress the expression of certain P53 target genes (42). In this study, we uncover another layer of interplay between P53 and BRD4. Intrigued by the strong correlation between P53 and BRD4 protein levels in liver cancer samples, we delineate that P53 lays significant impact on BRD4 protein stability through the P21–RB1 axis.

USP1 is a deubiquitinase of BRD4

With the biological significance of BRD4, regulation of its expression has been in the spotlight (12). The ubiquitination-proteasome system plays an important role in the regulation of BRD4 protein level. Several proteins were shown to regulate BRD4 ubiquitination, such as DUB3, SPOP, UCHL3, and USP22 (8–11, 15, 16). In this study, we identify USP1 as a deubiquitinase for BRD4 when delineating how P53 regulates

wise comparison as indicated. *D*, exogenous *CA9* was expressed in BRD4-KD cells. $6*10^5$ cells were then seeded into each 6-cm dish. Cell proliferation over 5 days was analyzed with cell counting. Fold of proliferation was normalized to that in control cells. Error bars denote SD of four biological replicates. *p* value was calculated by one-way ANOVA followed by pair-wise comparison as indicated. *E*, exogenous *CA9* was expressed in BRD4-KD cells. Thousand cells were then seeded into each 3.5 cm dish. Seventeen days later, cell colonies were stained with crystal violet.

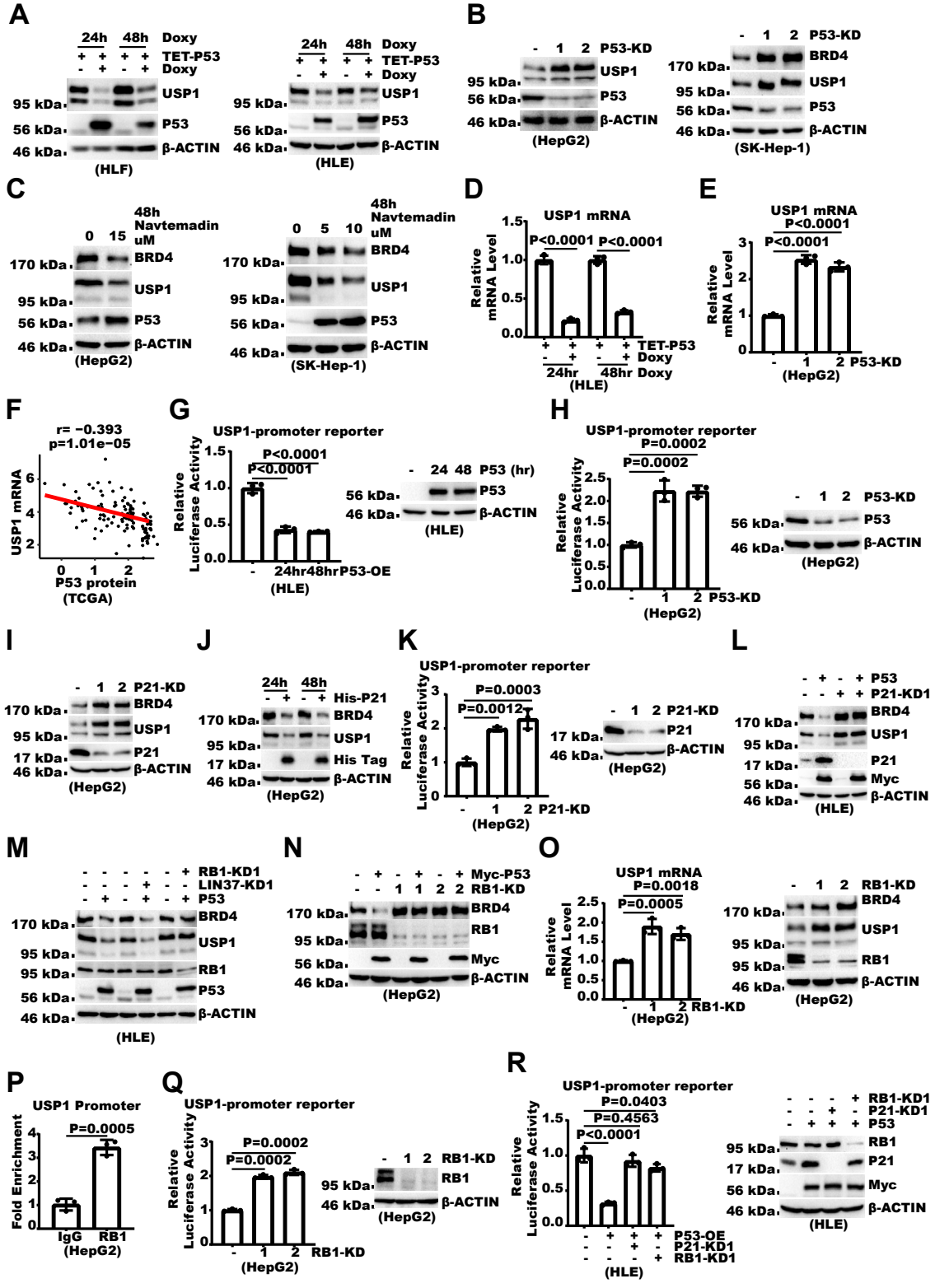

Figure 6. P53 represses USP1 and BRD4 expression through P21–RB1 axis. *A*, cells were transduced with lentivirus carrying tetracycline/doxycycline-inducible P53-expressing vector (TET-P53). After induction with 1 μg/ml doxycycline for 24 h and 48h, cells were collected for WB analysis. *B*, *TP53* was knocked-down with shRNA and WCL were analyzed with WB. *C*, HepG2 and SK-Hep-1 cells were treated with or without Navtemadin as indicated and then subjected to Western blot analyses. *D*, cells were transduced with lentivirus carrying doxycycline-inducible P53 expressing vector. After induction with 1 μg/ml doxycycline for 24 h and 48h, cells were collected for real-time RT-PCR analysis. Shown USP1 mRNA levels were normalized to β-actin. Error bars denote SD of three technical replicates. *p* values were calculated with one-way ANOVA followed by pair-wise comparison as indicated. *E*, *TP53* was knocked-down with shRNA and cells were analyzed with real-time RT-PCR. Shown USP1 mRNA levels were normalized to β-actin. Error bars denote SD of three technical replicates. *p* values were calculated with one-way ANOVA followed by pair-wise comparison as indicated. *F*, shown is linear regression analysis for correlation between P53 protein level and USP1 mRNA in 119 P53-WT patients as in TCGA RPPA dataset and RNA-Seq dataset, respectively. The "r" denotes Pearson correlation coefficient. *G*, luciferase reporter driven by USP1 promoter was stably expressed in HLE cells. P53 was overexpressed in these cells with

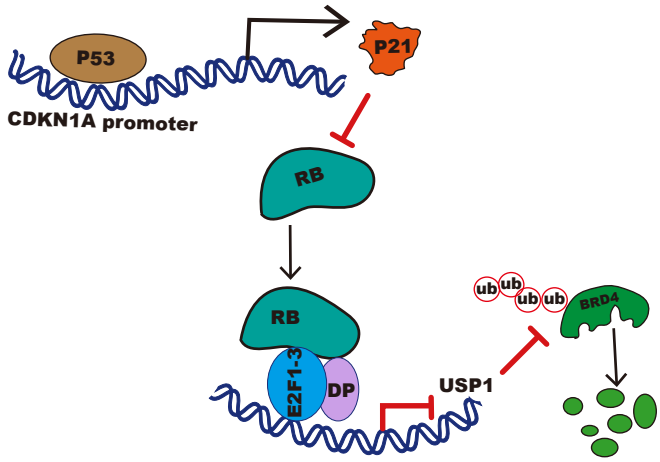

Figure 7. Working model. P53 promotes transcription of P21. P21 then prevents RB1 phosphorylation and inactivation. Active RB complex with E2F and DP, which then inhibits transcription of USP1. USP1 deubiquitinates and stabilizes BRD4 protein.

BRD4 protein stability in liver cancer. Consistently, we show that WDR48, a critical partner of USP1, is also important for the activity of USP1 on BRD4. Previous findings and ours altogether depict a landscape that BRD4 protein level is regulated by multiple pathways, which positions BRD4 for response to multiple upstream signals. This highlights BRD4 as a signaling hub which is consistent with its pleiotropic functions.

USP1 is an effector of the P53–P21–RB1 axis in liver cancer

Since identified as a deubiquitinase, USP1's prototypical function has been in the DNA damage repair process (43, 44). Recently, more and more studies are revealing the importance of USP1 in cancer biology (45). For example, in liver cancer, USP1 was reported to promote Wnt signaling pathway and ribosome biogenesis (46–48). Consistent with a function other than DNA repair, our pathway analysis showed USP1 mainly affected expression of genes in other cancer-related pathways in liver cancer cells (Fig. 5*A*). Nevertheless, how USP1 gets dysregulated in cancer remains unclear. Although overexpression of USP1 mRNA has long been recognized in cancer (49), studies on regulation of USP1 expression have been focused on its posttranslational modification, for example, ubiquitination by the APC complex (49). In this study, we uncover that transcription of USP1 is repressed by a master tumor suppressor gene, *TP53*. We revealed strong correlation between the P53 protein level and USP1 mRNA level. Meanwhile, USP1 mRNA level is significantly higher in P53-mutated samples than in P53-WT samples (Fig. 6). Since USP1 and BRD4 are critical for liver cancer malignancy as shown by previous studies and ours, this study highlights the USP1–BRD4 axis as a key downstream effector of P53.

Experimental procedures

Cell culture

Human hepatocellular carcinoma cells HepG2, HLF and HLE, as well as HEK-293T (human embryonic kidney cell) were from Dr Shuguo Sun's lab. SK-Hep-1 cells (Procell # CL-0212) were purchased from Procell. HepG2 and SK-Hep-1 are P53-WT while HLF and HLE carry P53-G244A according to The Cancer Cell Line Encyclopedia. HepG2, HLF and HLE, as well as HEK-293T were cultured in Dulbecco's Modified Eagle's Medium (Gibco #12800-082) supplemented with 10% fetal bovine serum(PAN, Germany. #ST30-3302). SK-Hep-1 cells were cultured in MEM (Procell #PM150410) supplemented with 10% fetal bovine serum. All cell lines were maintained in 37 °C incubator with 5% CO2. Cycloheximide (Sigma #C7698), MG132 (MCE # HY-13259), or doxycycline hyclate (MCE #HY-N0565B) was added to cell culture at a final concentration of 50 μg/ml, 25 μM, and 1 μg/ml respectively where indicated. ML-323 was added at 8 μM, 16 μM, or 32 μM as specified in the text.

Western blot

WB was performed as previously reported in detail (50). Following antibodies were used in WB: rabbit monoclonal anti-BRD4 (CST #13440), rabbit polyclonal anti-USP1 (Proteintech #14346-1-AP), WDR48 rabbit polyclonal anti-WDR48 (Proteintech # 16503-1-AP), rabbit monoclonal anti-β-ACTIN (ABclonal #AC026), mouse monoclonal anti-GAPDH (Abclonal #AC033), rabbit monoclonal anti- P21 (Proteintech #82669-2-RR), mouse monoclonal anti- P53 (Santa Cruz #SC-126), rabbit polyclonal anti- Myc Tag (Proteintech #16286-1-AP), mouse monoclonal anti- Myc Tag (Santa Cruz #SC-40), mouse monoclonal anti-hemagglutinin

lentivirus and luciferase activity was measured either 24 h or 48 h after virus transduction. On the *left* shows relative luciferase activity normalized to protein amount. Error bars denote SD of three biological replicates. *p* values were calculated with one-way ANOVA followed by pair-wise comparison. On the *right*, WCL were analyzed with WB to validate P53 overexpression. *H*, luciferase reporter driven by USP1 promoter was stably expressed in HepG2 cells. P53 was knocked-down in these cells and luciferase activity was measured. On the *left* shows relative luciferase activity normalized to protein amount. Error bars denote SD of three biological replicates. *p* values were calculated with one-way ANOVA followed by pair-wise comparison. On the *right*, WCL were analyzed with WB to validate P53 knockdown. *I*, *CDKN1A* (P21) was knocked-down in HepG2 cells with shRNA. WCL were analyzed with WB. *J*, P21 was overexpressed in HepG2 cells with lentivirus transduction. WCL were collected 24 h or 48 h later for WB analysis. *K*, luciferase reporter driven by USP1 promoter was stably expressed in HepG2 cells. *CDKN1A* was then knocked-down in these cells. On the *left*, luciferase activity was measured. On the *right*, WCL were analyzed with WB to confirm knockdown efficiency. Error bars denote SD of three biological replicates. *p* values were calculated with one-way ANOVA followed by pair-wise comparison. *L*, P53 was overexpressed in control or P21-KD cells. WCL were then analyzed with WB. *M*, RB1 or LIN37 was knocked-down in HLE cells and then *TP53* was expressed in these cells or control cells. WCL were then analyzed with WB. *N*, RB1 was knocked-down in HepG2 cells with separate shRNA and then *TP53* was expressed in these cells or control cells. WCL were then analyzed with WB. *O*, RB1 was knocked-down in HepG2 cells and then cells were analyzed with real-time RT-PCR (*left*) or WB (*right*). *P*, HepG2 cells were subject to Chromatin-IP analysis with RB1 antibody with IgG as control. *Q*, luciferase reporter driven by USP1 promoter was stably expressed in HepG2 cells. RB1 was knocked-down in these cells. On the *left*, luciferase activity was measured. On the *right*, WCL were analyzed with WB to validate knockdown efficiency. Error bars denote SD of three biological replicates. *p* values were calculated with one-way ANOVA followed by pair-wise comparison. *R*, luciferase reporter driven by USP1 promoter was stably expressed in HLE cells. RB1 or *CDKN1A* was then knocked-down in these cells. Afterward, P53 was expressed as indicated and luciferase activity was examined. CDK, cyclin-dependent kinase.

(HA) tag (Covance #MMS-101P), rabbit monoclonal anti-HA tag (CST #3724), rabbit polyclonal anti- RB1 (Proteintech # 10048-2-lg), horseradish peroxidase (HRP)–conjugated mouse monoclonal anti- GST tag (Proteintech #HRP-66001), mouse monoclonal anti- Ubiquitin (Santa Cruz #sc-8017), HRP-conjugated anti-FLAG (Sigma #A8592), HRP-conjugated Goat anti-rabbit IgG (H+L) secondary antibody (Abclonal #AS014), HRP-conjugated goat anti-mouse (H+L) secondary antibody (Abclonal #AS003).

In vitro *deubiquitination assay*

USP1 was cloned into pGEX-6P and GST-USP1 was purified with glutathione-conjugated agarose beads (GenScript #L00206) from BL21 Codon-plus *Escherichia coli* (second lab #EC1007) following the same procedure as we previously described (50). FLAG-WDR48 was transfected into 293T cells and was later immunopurified with anti-FLAG antibody–conjugated agarose beads (GenScript #L00432) and then eluted with 500 μg/ml 3x FLAG peptide. Myc-BRD4 was cotransfected with HA-ubiquitin into 293T cells and then immunoprecipitated with Myc-tag antibody (Santa Cruz #SC-40) and Protein-G–conjugated agarose beads (GenScript #L00209). Beads-bound Myc-BRD4 was then incubated with 0.8 μg GST-USP1 and 0.8 μg FLAG-WDR48 in BC50 buffer (20 mM Hepes PH7.5, 50 mM NaCl, 10% Glycerol) at 37 °C for 1 h. Reactant was analyzed with WB.

Luciferase assay

USP1-promoter was inserted in front of firefly luciferase coding sequence to make the pLenti-USP1-Luciferase. Lentivirus were produced with cotransfection of this plasmid together with psPAX2 and pMD2.G into 293T cells. Cells were transduced with lentivirus and selected with neomycin for 7 days. Luciferase activity was measured with "luciferase assay reagent" (Promega #E1483) following the manufacturer's recommendations. Briefly, 10 μl cell lysate was incubated with 40 μl of luciferase assay reagent in room temperature and loaded into black-well 96-well plate. Afterward, signal was read with a plate reader (CLARIO star plus).

Immunofluorescence

Cells were seeded on cover slide in 12-well plate and fixed with 4% paraformaldehyde in room temperature for 15 min. Afterward, cells were permeabilized with pre-cooled 0.5% TritonX-100 (dissolved in PBS) on ice for 5 min. After blocking with 1% bovine serum albumin, cells were incubated with primary antibodies at room temperature for 1 h. Primary antibodies used are anti-FLAG (Sigma #F7425), anti-Myc tag (Santa Cruz #SC-40), anti-BRD4 (CST #13440) and anti-USP1 (Proteintech #14346-1-AP). Slides were then incubated with secondary antibodies for 1 h at room temperature (Invitrogen #715-545-150, #711-585-152, and #711-545-152). Nuclei were counterstained with 1.5 μM 4′,6-diamidino-2-phenylindole for 5 min. Finally, cells were mounted onto a slide with mounting medium (Abcam #AB104135). Photos were taken with QImaging Retiga R6 Monochrome camera connected to Zeiss-A1 Axiovert A1 fluorescence microscopy equipped with 63 × oil object lens.

Inducible overexpression

P53 was cloned into pLenti-tetracycline-responsive element (TRE) vector (51). The vector contains a TRE and constitutively expressed rtTA3 activator as well puromycin resistance gene. P53 was inserted after the TRE. Lentivirus was produced by cotransfection of pLenti-TRE-P53, psPAX2, and pMD2.G into 293T cells. For inducible expression, cells were first transduced with lentivirus and then selected in 2 μg/ml puromycin. Cells were treated with 1 μg/ml doxycycline to induce expression.

Colony formation assay

Cells, typically 500 to 1000 in number as specified, were seeded into 3.5 cm dishes or 6-well plate. Culture medium was replenished once a week. After colonies become macroscopically visible, typically after 2 to 3 weeks, medium was discarded and cells were washed with PBS and fixed with crystal violet. Photos were taken with an EPSON photo scanner.

CCK8

Thousand cells were seeded into 96-well plate and let grow. Ten microliters of CCK8 (Beyotime #C0038) was added to each well containing 100 μl medium and incubated for 1 h. Then OD450 was measure on a plate reader (Multiskan GO, Thermo Fisher Scientific).

Xenograft study

Xenograft study was performed as we previously described (50). All animal experiments were performed following the institute guidelines and approved by the Ethics committee of Tongji Medical College. The mice were acclimated to the new environment for at least 1 week. Mice were housed in ventilated cages in a temperature-controlled room (21 ± 1 °C) with a 12 h light/12 h darkness cycle. Food and water were available ad libitum. 5×10^6 cells were resuspended in 100 μl PBS and matrigel (BD Biosciences #354248) 1:1 mixture. Cell suspension was then injected subcutaneously into flanks of 5 to 6 week-old male BALB/c nude mice (Beijing Vital River Laboratory Animal Technology). Tumor growth was measured with caliper every 3 to 7 days. Tumor volume was estimated by the formula 0.5*L*W*W (L means long diameter, W means short diameter). Mice were sacrificed before the estimated volume of any tumor reaches 1 cm^3.

Chromatin immunoprecipitation

Chromatin immunoprecipitation was performed as previously reported with modifications at the fixation step (50). Specifically, culture medium was discarded and cells were washed with PBS twice. Then cells were first fixed with 2.5 mM Disuccinimidyl glutarate (Alladin #D304655) in PBS for 45 min before fixation with formaldehyde. For IP step, primary antibodies used are anti-RB1 (Proteintech #10048-2-

Ig) with rabbit IgG (Proteintech #B900610) as control. Protein-A–conjugated magnetic beads (GenScript #L00464) were used to capture the antigen–antibody complex. Captured DNA was purified and analyzed with real-time PCR. Primers used are listed in the Table S3.

In vivo *ubiquitination assay*

In vivo ubiquitination assay was performed exactly as we described previously (50). For exogenous BRD4, BRD4 and Ubiquitin plasmids were cotransfected into 293T cells. BRD4 was then immunoprecipitated with tag antibodies. Alternatively, endogenous BRD4 was immunoprecipitated with BRD4 antibody. Immunoprecipitate was sufficiently washed and analyzed with WB.

Gene knockdown

shRNA-based gene knockdown was performed exactly as we previously described (50). DNA oligos were synthesized, annealed, and ligated into pLKO vector. Lentivirus was produced by cotransfecting pLKO, psPAX2, and pMD2.G into HEK-293T cells. Oligo sequences are listed in the Table S3.

Coimmunoprecipitation assay

Coimmunoprecipitation assay was performed exactly as we described previously (50). Antibodies used for IP are rabbit monoclonal anti-BRD4 (CST #13440), rabbit polyclonal anti-USP1 (PTG #14346-1-AP), mouse monoclonal anti- Myc Tag (Santa Cruz #SC-40), anti-FLAG-conjugated beads (Sigma #A2220 or GenScript #L00432).

GST pulldown assay

GST pulldown was performed as previously described (52). FLAG-BRD4 was transfected into 293T cell. Cells were lyzed in IPE150 buffer (20 mM Hepes pH 7.5, 150 mM NaCl, 0.5% NP40, 10% glycerol). Recombinant GST-USP1 from *E. coli* was added into cell lysate and incubated at 4 °C with rotation for 6 h. Glutathione-conjugated beads were added to precipitate GST–USP1/BRD4 complex. Afterward, the precipitate was analyzed with WB.

Real-time RT-PCR

Total RNA was extracted with TRNzol (TIANGEN #DP424) as recommended by the manufacturer. Reverse-transcription and Sybgreen-based realtime RT-PCR were performed as we previously reported (53). ReverTra Ace qPCR RT-Kit (Toyobo #FSQ-101), ThunderBird Syb Sybgreen Master Mix (Toyobo #QPK-201), and Bio-Rad CFX connect PCR machine were used. Used primers are listed in Table S3.

Densitometry analysis of WB result

Densitometry analysis of WB results with FIJI was performed exactly as we previously reported (52). Briefly, WB images were turned into 8 bit Gray and background was subtracted. Bands were manually circled out and densitometry was measured with the “measure” function in FIJI. Density from each sample was then normalized to the density of β-ACTIN or GAPDH from the same sample to get the relative level of each band. Afterward, the relative level of each sample was normalized to that of the control group.

Patient samples

Thirty pairs of primary hepatocellular carcinoma samples and paired tumor-adjacent samples were collected from surgery at Tongji Hospital affiliated with Huazhong University of Science and Technology. For tumor tissues, necrotic parts were removed. Tissues were frozen in liquid nitrogen upon collection until further analysis. To be analyzed by WB, tissues were grinded and sonicated in 1 x laemmli buffer. Use of these samples were approved by the Medical Ethics Committee of Tongji Medical College, Huazhong University of Science and Technology and abided by the Declaration of Helsinki principles.

Survival analysis and Kaplan–Meier plot

Patients were divided into "high" and "low" groups according to expression level of corresponding genes with median expression level as threshold unless otherwise indicated. "Survival" package in R was used for survival analysis and Kaplan–Meier plot.

Analysis of TCGA and CPTAC data

All RNA-seq STAR counts and RPPA data for TCGA hepatocellular carcinoma cohort were downloaded from Genomic Data Commons Data Portal. STAR counts were processed into Transcripts Per Million and RPPA data was used as is. P53 mutation status was based on the "Masked Somatic Mutation" information from TCGA. Mass spectrometry–based Protein expression data and accompanying clinic information for liver cancer patient were from a previous report as part of Clinical Proteomic Tumor Analysis Consortium and used as is (54).

RNA-sequencing

HepG2 cells were transduced with lentivirus carrying doxycycline inducible USP1-shRNA and BRD4-shRNA respectively cloned in TET-pLKO vector (55). Forty eight hours after lentivirus infection, cells were passaged into 6 cm dishes. Puromycin (InvivoGen #ANT-PR-1) was added at a final concentration of 1 μg/ml after 12 h. Cells were selected with puromycin for 3 days and then divided into two 6 cm dishes. The next day, cells were either left untreated or treated with 1 μg/ml doxycycline for 3 days. Culture medium was replenished every 2 days. Afterward, culture medium was discarded and cells were washed with PBS twice. Cells were then collected into TRNzol (TIANGEN Cat# DP424) in RNAase-free microcentrifuge tubes for subsequent RNA extraction. Total RNA was extracted as recommended by the manufacturer. Afterward, sample processing and sequencing were performed by BGI Inc. Briefly, messenger RNA was purified with magnetic beads conjugated with Oligo-dT and then fragmented with fragmentation buffer. Then first-strand cDNA was synthesized with random primer. After second-strand cDNA synthesis, A-tailing and RNA index adapters

were added. The cDNA fragments were amplified by PCR and products were purified by Ampure XP Beads. The product was then analyzed on the Agilent Technologies 2100 bioanalyzer for quality control. Afterward, the PCR product was heat-denatured and circularized by the splint oligo sequence to get the final library. The final library was amplified with Phi29 DNA Polymerase to make DNA nanoball which had more than 300 copies of one molecular. Pair-end 150 bases reads were generated on MGISEQ-2000RS platform (BGI).

Analysis of RNA-Seq data

Raw reads were first filtered with Trim-Galore and then aligned by STAR to human hg38 assembly with the Gencode V39 genome annotation. Alignments with MAPQ $>$ 10 were kept and then further filtered with 'RmDup' to remove PCR duplicate. Gene-level counts were generated with featureCounts and further analyzed for gene differential expression with DeSeq2 with default parameters. Volcano plot was generated with ggplot2 in R (4.2.1). Venn diagram for overlapping genes downregulated by both USP1-KD and BRD4-KD was generated with ggVenndiagram package in R (4.2.1). Fisher exact test was used to test whether overlapping between the two groups of genes was statistically significant.

GSEA analysis

Genes are first sorted by the "shrinked Log2FC" (log2 fold change statistically adjusted) as calculated by DESeq2. GSEA analysis was performed as we reported (53). In brief, R package "fgsea" and hallmark gene sets from Human MSigDB Collections were used. *p* values were obtained by permuting the gene set 1000 times.

Statistical analysis

To compare the difference in BRD4 or USP1 protein levels between paired normal and cancer liver tissues, two-sided paired Welch's *t* test was used. Linear regression analysis and Pearson correlation analysis were performed in R (4.2.1) with basic functions. To statistically analyze overlapping between BRD4-regulated genes and USP1-regulated genes in RNA-Seq, Fisher exact test was used. *p* values (or p-adjusted for multiple comparison) less than 0.05 were deemed significant. Scatter plots, boxplots, and volcano plots were generated with "ggplot2" and/or "ggbeeswarm" packages in R (4.2.1). Bar graphs were generated in Graphpad Prism 8. Sample sizes were specified in figure legends where applicable. All error bars denote SD.

Data availability

The data that support the findings of this study are available in the manuscript or the supporting information. In addition, Raw data from RNA-Seq have been deposited to Gene Expression Omnibus (GEO) under accession number GSE243936.

Supporting information—This article contains supporting information.

Author contributionss—N. L., T. S., and L. S. conceptualization; N. L., E. Z., Z. L., S. L., X. Z., and Q. Z. methodology; N. L., E. Z., Z. L., S. L., X. Z., Q. K., Q. Z., W. L., Y. W., and H. G. investigation; N. L., E. Z., Z. L., S. L., X. Z., Q. K., Q. Z., W. L., Y. W., and H. G. validation; N. L., T. S., and L. S. visualization; N. L., T. S., and L. S. writing–original draft; T. S. and L. S. writing–review & editing; T. S. supervision; E. Z., T. S., and L. S. funding acquisition.

Funding and additional information—This work was supported by grants from the National Natural Science Foundation of China (32071296, 32371320, and 31871284 to L. S., 31971149 and 31800641 to T. S., 81902839 to E. Z.) and Natural Science Foundation of Hubei Province of China (2022CFB251 to T. S.).

Conflict of interest—The authors declare that they have no conflicts of interest with the contents of this article.

Abbreviations—The abbreviations used are: BRD4, Bromodomain containing 4; CA9, carbonic anhydrase 9; CCK-8, Cell Counting Kit-8; CDK, cyclin-dependent kinase; GSEA, gene set enrichment analysis; HA, hemagglutinin; HRP, horseradish peroxidase; IP, immunoprecipitation; LIN37, lin-37 DREAM MuvB core complex component; NDUFA4L2, NDUFA4 mitochondrial complex associated like 2; RB1, RB transcriptional corepressor 1; RPPA, reverse phase protein array; SLC2A3, solute carrier family 2 member 3; SPOP, speckle type BTB/POZ protein; TCGA, The Cancer Genome Atlas; TNS4, tensin 4; TP53, tumor protein p53; TRE, tetracycline-responsive element; UCHL3, ubiquitin C-terminal hydrolase L3; USP, Ubiquitin Specific Peptidase; WB, Western Blot; WCL, whole cell lysate.

References

1. Sung, H., Ferlay, J., Siegel, R. L., Laversanne, M., Soerjomataram, I., Jemal, A., *et al.* (2021) Global cancer statistics 2020: GLOBOCAN estimates of incidence and mortality worldwide for 36 cancers in 185 countries. *CA Cancer J. Clin.* **71**, 209–249
2. Demir, T., Lee, S. S., and Kaseb, A. O. (2021) Systemic therapy of liver cancer. *Adv. Cancer Res.* **149**, 257–294
3. Donati, B., Lorenzini, E., and Ciarrocchi, A. (2018) BRD4 and Cancer: going beyond transcriptional regulation. *Mol. Cancer* **17**, 164
4. Liang, D., Yu, Y., and Ma, Z. (2020) Novel strategies targeting bromodomain-containing protein 4 (BRD4) for cancer drug discovery. *Eur. J. Med. Chem.* **200**, 112426
5. Belkina, A. C., and Denis, G. V. (2012) BET domain co-regulators in obesity, inflammation and cancer. *Nat. Rev. Cancer* **12**, 465–477
6. French, C. A., Miyoshi, I., Kubonishi, I., Grier, H. E., Perez-Atayde, A. R., and Fletcher, J. A. (2003) BRD4-NUT fusion oncogene: a novel mechanism in aggressive carcinoma. *Cancer Res.* **63**, 304–307
7. Crawford, N. P., Alsarraj, J., Lukes, L., Walker, R. C., Officewala, J. S., Yang, H. H., *et al.* (2008) Bromodomain 4 activation predicts breast cancer survival. *Proc. Natl. Acad. Sci. U. S. A.* **105**, 6380–6385
8. Zhang, P., Wang, D., Zhao, Y., Ren, S., Gao, K., Ye, Z., *et al.* (2017) Intrinsic BET inhibitor resistance in SPOP-mutated prostate cancer is mediated by BET protein stabilization and AKT-mTORC1 activation. *Nat. Med.* **23**, 1055–1062
9. Janouskova, H., El Tekle, G., Bellini, E., Udeshi, N. D., Rinaldi, A., Ulbricht, A., *et al.* (2017) Opposing effects of cancer-type-specific SPOP mutants on BET protein degradation and sensitivity to BET inhibitors. *Nat. Med.* **23**, 1046–1054
10. Dai, X., Gan, W., Li, X., Wang, S., Zhang, W., Huang, L., *et al.* (2017) Prostate cancer-associated SPOP mutations confer resistance to BET inhibitors through stabilization of BRD4. *Nat. Med.* **23**, 1063–1071
11. Jin, X., Yan, Y., Wang, D., Ding, D., Ma, T., Ye, Z., *et al.* (2018) DUB3 promotes BET inhibitor resistance and cancer progression by deubiquitinating BRD4. *Mol. Cell* **71**, 592–605

12. Liu, N., Ling, R., Tang, X., Yu, Y., Zhou, Y., and Chen, D. (2022) Post-translational modifications of BRD4: therapeutic targets for tumor. *Front. Oncol.* **12**, 847701
13. Lange, S. M., Armstrong, L. A., and Kulathu, Y. (2022) Deubiquitinases: from mechanisms to their inhibition by small molecules. *Mol. Cell* **82**, 15–29
14. Berndsen, C. E., and Wolberger, C. (2014) New insights into ubiquitin E3 ligase mechanism. *Nat. Struct. Mol. Biol.* **21**, 301–307
15. Wang, W., Tang, Y. A., Xiao, Q., Lee, W. C., Cheng, B., Niu, Z., *et al.* (2021) Stromal induction of BRD4 phosphorylation results in chromatin remodeling and BET inhibitor resistance in colorectal cancer. *Nat. Commun.* **12**, 4441
16. Yan, R., Chu, J., Zhou, Y., Shan, W., Hu, Y., Lin, M., *et al.* (2021) Ubiquitin-specific protease 22 ameliorates chronic alcohol-associated liver disease by regulating BRD4. *Pharmacol. Res.* **168**, 105594
17. Bykov, V. J. N., Eriksson, S. E., Bianchi, J., and Wiman, K. G. (2018) Targeting mutant p53 for efficient cancer therapy. *Nat. Rev. Cancer* **18**, 89–102
18. Sullivan, K. D., Galbraith, M. D., Andrysik, Z., and Espinosa, J. M. (2018) Mechanisms of transcriptional regulation by p53. *Cell Death Differ.* **25**, 133–143
19. Engeland, K. (2022) Cell cycle regulation: p53-p21-RB signaling. *Cell Death Differ.* **29**, 946–960
20. Fischer, M., Schade, A. E., Branigan, T. B., Muller, G. A., and DeCaprio, J. A. (2022) Coordinating gene expression during the cell cycle. *Trends Biochem. Sci.* **47**, 1009–1022
21. Uxa, S., Bernhart, S. H., Mages, C. F. S., Fischer, M., Kohler, R., Hoffmann, S., *et al.* (2019) DREAM and RB cooperate to induce gene repression and cell-cycle arrest in response to p53 activation. *Nucleic Acids Res.* **47**, 9087–9103
22. Chen, Y. R., Ouyang, S. S., Chen, Y. L., Li, P., Xu, H. W., and Zhu, S. L. (2020) BRD4/8/9 are prognostic biomarkers and associated with immune infiltrates in hepatocellular carcinoma. *Aging (Albany NY)* **12**, 17541–17567
23. Tsang, F. H., Law, C. T., Tang, T. C., Cheng, C. L., Chin, D. W., Tam, W. V., *et al.* (2019) Aberrant super-enhancer landscape in human hepatocellular carcinoma. *Hepatology* **69**, 2502–2517
24. Chuang, K. T., Wang, S. N., Hsu, S. H., and Wang, L. T. (2021) Impact of bromodomain-containing protein 4 (BRD4) and intestine-specific homeobox (ISX) expression on the prognosis of patients with hepatocellular carcinoma' for better clarity. *Cancer Med.* **10**, 5545–5556
25. Zhang, P., Dong, Z., Cai, J., Zhang, C., Shen, Z., Ke, A., *et al.* (2015) BRD4 promotes tumor growth and epithelial-mesenchymal transition in hepatocellular carcinoma. *Int. J. Immunopathol. Pharmacol.* **28**, 36–44
26. Yu, B., Zhou, S., Long, D., Ning, Y., Yao, H., Zhou, E., *et al.* (2022) DDX55 promotes hepatocellular carcinoma progression by interacting with BRD4 and participating in exosome-mediated cell-cell communication. *Cancer Sci.* **113**, 3002–3017
27. Ghandi, M., Huang, F. W., Jane-Valbuena, J., Kryukov, G. V., Lo, C. C., McDonald, E. R., 3rd, *et al.* (2019) Next-generation characterization of the cancer cell line Encyclopedia. *Nature* **569**, 503–508
28. Rahman, S., Sowa, M. E., Ottinger, M., Smith, J. A., Shi, Y., Harper, J. W., *et al.* (2011) The Brd4 extraterminal domain confers transcription activation independent of pTEFb by recruiting multiple proteins, including NSD3. *Mol. Cell Biol.* **31**, 2641–2652
29. Cohn, M. A., Kowal, P., Yang, K., Haas, W., Huang, T. T., Gygi, S. P., *et al.* (2007) A UAF1-containing multisubunit protein complex regulates the Fanconi anemia pathway. *Mol. Cell* **28**, 786–797
30. Liang, F., Miller, A. S., Longerich, S., Tang, C., Maranon, D., Williamson, E. A., *et al.* (2019) DNA requirement in FANCD2 deubiquitination by USP1-UAF1-RAD51AP1 in the Fanconi anemia DNA damage response. *Nat. Commun.* **10**, 2849
31. Liang, Q., Dexheimer, T. S., Zhang, P., Rosenthal, A. S., Villamil, M. A., You, C., *et al.* (2014) A selective USP1-UAF1 inhibitor links deubiquitination to DNA damage responses. *Nat. Chem. Biol.* **10**, 298–304
32. Becker, H. M. (2020) Carbonic anhydrase IX and acid transport in cancer. *Br. J. Cancer* **122**, 157–167
33. Di-Luoffo, M., Pirenne, S., Saandi, T., Loriot, A., Gerard, C., Dauguet, N., *et al.* (2021) A mouse model of cholangiocarcinoma uncovers a role for Tensin-4 in tumor progression. *Hepatology* **74**, 1445–1460
34. Muharram, G., Sahgal, P., Korpela, T., De Franceschi, N., Kaukonen, R., Clark, K., *et al.* (2014) Tensin-4-dependent MET stabilization is essential for survival and proliferation in carcinoma cells. *Dev. Cell* **29**, 421–436
35. Liao, Y. C., and Lo, S. H. (2021) Tensins - emerging insights into their domain functions, biological roles and disease relevance. *J. Cell Sci.* **134**, jcs254029
36. Lucarelli, G., Loizzo, D., Franzin, R., Battaglia, S., Ferro, M., Cantiello, F., *et al.* (2019) Metabolomic insights into pathophysiological mechanisms and biomarker discovery in clear cell renal cell carcinoma. *Expert Rev. Mol. Diagn.* **19**, 397–407
37. Ancey, P. B., Contat, C., and Meylan, E. (2018) Glucose transporters in cancer - from tumor cells to the tumor microenvironment. *FEBS J.* **285**, 2926–2943
38. Rego, M. A., Harney, J. A., Mauro, M., Shen, M., and Howlett, N. G. (2012) Regulation of the activation of the Fanconi anemia pathway by the p21 cyclin-dependent kinase inhibitor. *Oncogene* **31**, 366–375
39. Wu, S. Y., Lee, A. Y., Lai, H. T., Zhang, H., and Chiang, C. M. (2013) Phospho switch triggers Brd4 chromatin binding and activator recruitment for gene-specific targeting. *Mol. Cell* **49**, 843–857
40. Kfoury, N., Qi, Z., Prager, B. C., Wilkinson, M. N., Broestl, L., Berrett, K. C., *et al.* (2021) Brd4-bound enhancers drive cell-intrinsic sex differences in glioblastoma. *Proc. Natl. Acad. Sci. U. S. A.* **118**, e2017148118
41. Sakamaki, J. I., Wilkinson, S., Hahn, M., Tasdemir, N., O'Prey, J., Clark, W., *et al.* (2017) Bromodomain protein BRD4 is a transcriptional repressor of autophagy and lysosomal function. *Mol. Cell* **66**, 517–532
42. Latif, A. L., Newcombe, A., Li, S., Gilroy, K., Robertson, N. A., Lei, X., *et al.* (2021) BRD4-mediated repression of p53 is a target for combination therapy in AML. *Nat. Commun.* **12**, 241
43. Huang, T. T., Nijman, S. M., Mirchandani, K. D., Galardy, P. J., Cohn, M. A., Haas, W., *et al.* (2006) Regulation of monoubiquitinated PCNA by DUB autocleavage. *Nat. Cell Biol.* **8**, 339–347
44. Nijman, S. M., Huang, T. T., Dirac, A. M., Brummelkamp, T. R., Kerkhoven, R. M., D'Andrea, A. D., *et al.* (2005) The deubiquitinating enzyme USP1 regulates the Fanconi anemia pathway. *Mol. Cell* **17**, 331–339
45. Antonenko, S., Zavelevich, M., and Telegeev, G. (2023) The role of USP1 deubiquitinase in the pathogenesis and therapy of cancer. *Acta Biochim. Pol.* **70**, 219–231
46. Chen, Z., Ma, Y., Guo, Z., Song, D., Chen, Z., and Sun, M. (2022) Ubiquitin-specific protease 1 acts as an oncogene and promotes lenvatinib efficacy in hepatocellular carcinoma by stabilizing c-kit. *Ann. Hepatol.* **27**, 100669
47. Li, Y., Xu, Y., Gao, C., Sun, Y., Zhou, K., Wang, P., *et al.* (2020) USP1 maintains the survival of liver circulating tumor cells by deubiquitinating and stabilizing TBLR1. *Front. Oncol.* **10**, 554809
48. Liao, Y., Shao, Z., Liu, Y., Xia, X., Deng, Y., Yu, C., *et al.* (2021) USP1-dependent RPS16 protein stability drives growth and metastasis of human hepatocellular carcinoma cells. *J. Exp. Clin. Cancer Res.* **40**, 201
49. Garcia-Santisteban, I., Peters, G. J., Giovannetti, E., and Rodriguez, J. A. (2013) USP1 deubiquitinase: cellular functions, regulatory mechanisms and emerging potential as target in cancer therapy. *Mol. Cancer* **12**, 91
50. Song, T., Zou, Q., Yan, Y., Lv, S., Li, N., Zhao, X., *et al.* (2021) DOT1L O-GlcNAcylation promotes its protein stability and MLL-fusion leukemia cell proliferation. *Cell Rep.* **36**, 109739
51. Lv, S., Zhao, X., Ma, X., Zou, Q., Li, N., Yan, Y., *et al.* (2022) Efficient and reversible Cas13d-mediated knockdown with an all-in-one lentivirus-vector. *Front. Bioeng. Biotechnol.* **10**, 960192
52. Lv, S., Zhao, X., Zhang, E., Yan, Y., Ma, X., Li, N., *et al.* (2022) Lysine demethylase KDM1A promotes cell growth via FKBP8-BCL2 axis in hepatocellular carcinoma. *J. Biol. Chem.* **298**, 102374
53. Song, T., Lv, S., Ma, X., Zhao, X., Fan, L., Zou, Q., *et al.* (2023) TRIM28 represses renal cell carcinoma cell proliferation by inhibiting TFE3/KDM6A-regulated autophagy. *J. Biol. Chem.* **299**, 104621
54. Gao, Q., Zhu, H., Dong, L., Shi, W., Chen, R., Song, Z., *et al.* (2019) Integrated proteogenomic characterization of HBV-related hepatocellular carcinoma. *Cell* **179**, 561–577
55. Wiederschain, D., Wee, S., Chen, L., Loo, A., Yang, G., Huang, A., *et al.* (2009) Single-vector inducible lentiviral RNAi system for oncology target validation. *Cell Cycle* **8**, 498–504
56. Castella, M., Jacquemont, C., Thompson, E. L., Yeo, J. E., Cheung, R. S., Huang, J. W., *et al.* (2015) FANCI regulates recruitment of the FA core complex at sites of DNA damage independently of FANCD2. *PLoS Genet.* **11**, e1005563